PROCEEDINGS A

royalsocietypublishing.org/journal/rspa

Research

Cite this article: Zhang Q, Sharma U, Dennis JA, Scifo A, Kuitems M, Büntgen U, Owens MJ, Dee MW, Pope BJS. 2022 Modelling cosmic radiation events in the tree-ring radiocarbon record. *Proc. R. Soc. A* **478**: 20220497. https://doi.org/10.1098/rspa.2022.0497

Received: 18 July 2022
Accepted: 3 October 2022

Subject Areas:
computer modelling and simulation, atmospheric science, astrophysics

Keywords:
radiocarbon, Miyake events, carbon cycle, atmospheric carbon, solar flares

Author for correspondence:
Benjamin J. S. Pope
e-mail: b.pope@uq.edu.au

Downloaded from https://royalsocietypublishing.org/ on 31 October 2022

Modelling cosmic radiation events in the tree-ring radiocarbon record

Qingyuan Zhang[1], Utkarsh Sharma[1], Jordan A. Dennis[1], Andrea Scifo[2], Margot Kuitems[2], Ulf Büntgen[3,4,5,6], Mathew J. Owens[7], Michael W. Dee[2] and Benjamin J. S. Pope[1,8]

[1]School of Mathematics and Physics, University of Queensland, St Lucia, Queensland 4072, Australia
[2]Centre for Isotope Research, University of Groningen, Groningen, The Netherlands
[3]Department of Geography, University of Cambridge, Cambridge CB2 3EN, UK
[4]Global Change Research Institute (CzechGlobe), Czech Academy of Sciences, 60300 Brno, Czech Republic
[5]Department of Geography, Faculty of Science, Masaryk University, 61137 Brno, Czech Republic
[6]Swiss Federal Research Institute (WSL), 8903 Birmensdorf, Switzerland
[7]Department of Meteorology, University of Reading, Earley Gate, PO Box 243, Reading RG6 6BB, UK
[8]Centre for Astrophysics, University of Southern Queensland, West Street, Toowoomba, Queensland 4350, Australia

QZ, 0000-0002-0906-8533; US, 0000-0002-0771-8109; JAD, 0000-0001-8125-6494; AS, 0000-0002-7174-3966; MK, 0000-0002-8803-2650; UB, 0000-0002-3821-0818; MJO, 0000-0003-2061-2453; MWD, 0000-0002-3116-453X; BJSP, 0000-0003-2595-9114

Annually resolved measurements of the radiocarbon content in tree-rings have revealed rare sharp rises in carbon-14 production. These 'Miyake events' are likely produced by rare increases in cosmic radiation from the Sun or other energetic astrophysical sources. The radiocarbon produced is not only circulated through the Earth's atmosphere and oceans, but also absorbed by the biosphere and locked in the annual

THE ROYAL SOCIETY PUBLISHING

© 2022 The Author(s) Published by the Royal Society. All rights reserved.

Downloaded from https://royalsocietypublishing.org/ on 31 October 2022

growth rings of trees. To interpret high-resolution tree-ring radiocarbon measurements therefore necessitates modelling the entire global carbon cycle. Here, we introduce '`ticktack`' (https://github.com/SharmaLlama/ticktack/), the first open-source Python package that connects box models of the carbon cycle with modern Bayesian inference tools. We use this to analyse all public annual ^{14}C tree data, and infer posterior parameters for all six known Miyake events. They do not show a consistent relationship to the solar cycle, and several display extended durations that challenge either astrophysical or geophysical models.

1. Introduction

Radiocarbon dating is used to accurately determine the age of samples of biological material, and is a fundamental tool of modern archaeology [1,2]. Thermal neutrons produced by cosmic rays interact with ^{14}N atoms in the upper atmosphere to produce radioactive ^{14}C , or radiocarbon, which filters across the carbon cycle through the atmosphere, biosphere, and marine environments. Libby *et al.* [3] demonstrated that the ratio of ^{14}C to stable carbon isotope abundances is approximately constant in the atmosphere over time: while living organisms continually replenish ^{14}C from the atmosphere, in dead organic matter this radiocarbon decays with a 5700-year half life, and therefore can be used as a clock to date archaeological and palaeontological samples.

In detail, this picture is complicated by variations in the radiocarbon production rate. The most relevant source of variation in the context of this work is from the activity cycle of the Sun. At low points in solar activity, reduced magnetic shielding means that the cosmic ray flux at Earth is increased [4]; but also, shocks ahead of solar coronal mass ejections can accelerate energetic particles that produce radiocarbon in Earth's atmosphere. As a result, radiocarbon measurements are not only important tools for archaeology, but also for historical studies of space weather, solar and geomagnetic activity and the Earth's climate dynamics [5].

For many species, tree-rings can be dated to the exact year of their formation, the science of dendrochronology. Radiocarbon in tree-rings, appropriately adjusted for radioactive decay, therefore offers a detailed record of radiocarbon concentrations over time. The existence of variation from one year to the next was first shown by de Vries [6]. Using measurements on North American bristlecone pine, Suess [7] revealed the scale of radiocarbon fluctuations over millennial time scales, demonstrating the necessity for a 'calibration curve' for archaeological dating. Such curves have attained increasing sophistication over time, and have in the last decade attained high precision and annual resolution, for example IntCal13 [8] and IntCal20 [9–11].

These newly detailed curves revealed the long-suspected astrophysical influence of the solar activity cycle on modulating radiocarbon production in individual solar cycles [12]. They also yielded a surprise: Miyake *et al.* [13] discovered in Japanese cedar tree-rings a sudden single-year jump in radiocarbon concentration around 774 CE. This was followed shortly by the discovery of another spike in tree-rings from 993 CE [14], and further such spikes have been found in 660 BCE [15], 5259 BCE [16], 5410 BCE [17] and 7176 BCE [16], for a total of six well-studied and accepted radiocarbon spikes. These are often known as 'Miyake events', after their first discoverer. Other spikes have been claimed from some tree-ring samples, but not replicated globally: one in 800 BCE [18], and claimed but refuted in 3372 BCE [19,20]. Several small events are also proposed in 1052 CE, and 1261, 1268 and 1279 CE by Brehm *et al.* [21] and Miyahara *et al.* [22].

Detailed study of these events is important to determine their origin. Better data are available for the two events in the Common Era, showing that the events of 774 and 993 CE are globally coherent, including many trees in both the Northern and Southern Hemispheres [23]. Meanwhile, although the other events show sharp single-year rises, the event of 660 BCE has a prolonged rise over a couple of years, which could be due to a prolonged production or a succession of events [24]. For comparison, a decade-long rise in 5480 BCE, less than a century before the single-year

Downloaded from https://royalsocietypublishing.org/ on 31 October 2022

rise in 5410 BCE, is ascribed by multiradionuclide evidence to an unusual grand solar minimum of very great depth and short duration [25,26]. No other sharp rises in Δ^{14}C so far detected have shown evidence of substructure in time.

Miyake events offer archaeologists a sharp radiocarbon signal, synchronized across the Earth, which can be used to achieve single-year dates for tree-rings in samples otherwise beyond the reach of dendrochronology [27]. For example, the historically significant eruption of the Changbaishan volcano can be dated to 946 CE [28,29]. By dating the Uyghur site of Por-Bajin in Russia to exactly 777 CE , it can be identified as a monastery built under the Uyghur Khaganate's short-lived conversion to Manichaeism [30]. These data have been most revolutionary for Viking Age archaeology. The 774 CE event dates finds at Ribe, Denmark, and anchors interpretation of their trade networks [31], while the 993 CE event securely dates the L'Anse aux Meadows settlement to 1021 CE—the first evidence of European settlement in the Americas [32].

The sharp rise in radiation, with a simultaneous global onset, indicates that Miyake events are of astrophysical origin, for which a variety of explanations have been offered (thoroughly reviewed in [33]). Dying stars and their remnants are known to produce extremely intense bursts of radiation, and are *prima facie* reasonable astrophysical sources. For instance, a sharp burst of radiation could have been delivered by a Galactic gamma-ray burst [34,35] or nearby supernova, though astronomical evidence of these is so far lacking. Dee *et al.* [36] have failed to find evidence of a radiocarbon rise associated with any of the known historical supernovae, while Terrasi *et al.* [37] find a 2σ increase in radiocarbon in 1055 CE after the Crab supernova. An alternative proposal considers a magnetar burst from a nearby magnetized neutron star [38], which is energetically plausible—but no sufficiently nearby or active neutron star is yet known from conventional astronomical observations. Pavlov *et al.* [39] and Pavlov *et al.* [40] have suggested prolonged events like 660 BCE and 5480 BCE are the result of enhanced Galactic cosmic ray flux over several years after the heliosphere is compressed by dense clouds in the interstellar medium. Closer to home, Liu *et al.* [41] suggest the ^{14}C could be deposited into the atmosphere directly by a passing comet; this interpretation is rejected by Usoskin & Kovaltsov [42], who argue that such a comet would need to have been of a size ($\gtrsim$100 km) that would have devastated the Earth.

The wide consensus of the literature is that these events have a solar origin, beginning with Melott & Thomas [43]; Usoskin *et al.* [44]. For example, the events could represent a solar magnetic collapse, a very brief grand solar minimum, with the reduced heliospheric shielding exposing the Earth to an increase in Galactic cosmic rays [45]. Alternatively, and more popular in the literature, the Miyake events could represent the extreme tail of a distribution of solar flares continuous with those that are observed astrophysically on the modern Sun and other solar-like stars. We are fortunate that ^{14}C is not the only cosmogenic isotope that can trace these events: we see evidence of the 774 CE and 993 CE events in time series of ^{10}Be and ^{36}Cl from ice cores [46,47], and because the production of these isotopes depends on input particle energy, they can be used to infer a particle energy spectrum similar to solar energetic protons [48]. Only the most energetic particles produce ^{10}Be , but ^{36}Cl is expected to be produced at comparatively low energies and may therefore shed light on other events as well [49]. Extreme solar flares or emissions are plausible astrophysically: based on the findings of the *Kepler* Space Telescope [50], G dwarf stars (like the Sun) are thought to produce superflares every few hundred to few thousand years [51], even old and slowly rotating stars [52,53].

Nevertheless, even in light of the uncertainties in particle flux from the existing literature, an event like the 774 CE event would need to be more than an order of magnitude larger than even the Carrington event, the most significant coronal mass ejection and accompanying geomagnetic storm ever observed in the instrumental era of science [54]. By considering possible beaming angles and uncertainties in models of the carbon cycle, Neuhäuser & Hambaryan [55] argue that the 774 CE event might be implausibly huge to be a single solar superflare. The solar proton event of 1956 produced an estimated 3.04×10^6 atoms/cm^{-2} of ^{14}C [56]; depending on assumptions about its flare class and spectral hardness, the 774 CE event could correspond to an X-ray flare as bright as X1800, nearly two orders of magnitude larger than any previously observed [57].

Downloaded from https://royalsocietypublishing.org/ on 31 October 2022

Meanwhile, ice core nitrate records at 774 CE and 993 CE do not show any hint of a signal from extreme solar activity [58,59]. At least some superflares observed from other stars are known in fact to originate from unresolved M dwarf binary companions [60], which are much more active than G dwarfs like the Sun and, because we do not have such a companion ourselves, could not explain the radiocarbon bursts. Extreme geomagnetic storms preferentially occur around the maxima of the solar cycle [61]. While the historical data on solar energetic particle events is far more limited, it is reasonable to assume they follow a similar pattern [62], as both result from energetic coronal mass ejections. Thus if Miyake events occur preferentially at solar maxima, this would support a solar origin. The radiocarbon data themselves contain the 11-year solar cycle, and several attempts have been made to determine its phase at the time of a Miyake event [15,21,63–65]. In this paper, we will attempt a similar inference.

Unfortunately, there is fairly limited evidence in written historical accounts for unusual astronomical phenomena coinciding with the radiocarbon spikes (for a comprehensive account, see [66]). The Anglo-Saxon Chronicle reports a 'red crucifix, after sunset' in 774 CE [67]; if this is an aurora, this is consistent with a massive solar flare, but it has been argued that the 'crucifix' is simply a lunar optical halo (Neuhäuser & Neuhäuser [68], an interpretation rejected by Hayakawa *et al.* [69]). An aurora is also reported in 775 CE from the Chinese chronicle Jiutangshu [70]. It remains the case that other historical records have not conclusively been shown to refer to aurorae in the year around this event.

Understanding the long-term behaviour of solar activity is of current interest in astrophysics. A grand minimum in stellar activity has only been observed in one star other than the Sun [71,72], and the Sun's own dynamo may be unusual. Solar-like stars are born rapidly rotating and very magnetically active, and their magnetized winds slow their rotation as they age—so that the age of solar-like stars might be inferred from appropriately calibrated relations of 'gyrochronology' [73]. No single gyrochronology relation, however, fits the rotation periods of large samples of stars determined with *Kepler* [74]. The emerging consensus is that weakened magnetic braking in older stars causes the activity to diminish without commensurate reduction in rotation periods [75–77], and this may be caused by a transition occurring at Rossby numbers of order unity between a fast and a slow type of stellar magnetic dynamo [78,79]. Remarkably, not only is the Sun less active than most solar-like stars [80], it so happens that our own Sun is at about the age and Rossby number of the proposed transition—so that it may be atypical of field stars generally, and long-term time series of its activity are of broad relevance in astrophysics.

If a Miyake event were to occur today, the sudden and dramatic rise in cosmic radiation could be devastating to the biosphere and technological society. It is therefore concerning that we have little understanding of how to predict their occurrence or effects. A solar proton event orders of magnitude more powerful than any previously observed could cause an 'internet apocalypse' of prolonged outages by damaging submarine cables and satellites [81]. The direct effects of energetic particles could even harm the health of passengers in high-altitude aircraft [82–84]. It is also likely that the 774 CE event would have caused a approximately 8.5% depletion in global ozone coverage, with a significant but not catastrophic effect on weather [59]. The origin and physics of these radiocarbon spikes are therefore important not just for astronomers and archaeologists, but for risk planning and mitigation in general society.

(a) Carbon cycle models

A very short pulse of radiation striking the atmosphere leads to a sharp rise (approx. 1 year) in measured $\Delta^{14}C$ and slow decay (approximately decade timescale) as the new radiocarbon is filtered through the global carbon cycle, finding its way into the biosphere, oceans, and sediments. Therefore to interpret radiocarbon time-series astrophysically, it is necessary to model this carbon cycle. The most popular way of doing this is using a Carbon Box Model (CBM; [85–89]), in which the global carbon budget is partitioned between discrete reservoirs (e.g. the atmosphere, oceans and biota, or subdivisions thereof). It is also common to include effects of atmospheric circulation or geochemistry in other areas of geoscience and planetary science (e.g. [90,91]), but on the

Downloaded from https://royalsocietypublishing.org/ on 31 October 2022

timescales and sensitivities relevant to Miyake events, these reservoirs are assumed to be coupled to one another linearly. This leads to a system of first-order ordinary differential equations (ODEs): a diffusion process, with an inhomogeneous driving term for atmospheric production.

While CBMs are essential for relating tree-ring time series to production rates, none of those models applied to Miyake events in the literature are available open-source. As a consequence, different analyses contain model-dependent systematic effects that are hard to reproduce or calibrate.

In this paper, we introduce a fast Python framework for carbon box models, ticktack (https://sharmallama.github.io/ticktack).[1] The framework is designed to be flexible, allowing arbitrary box models to be specified and modified. This is implemented in the high-performance Google JAX library [92], which supports just-in-time compilation, automatic differentiation, and code deployment to graphics processing unit (GPU)s. This code interfaces with the popular Bayesian inference packages `emcee` [93] and JAXNS [94]. We use this to reproduce several recent CBMs applied to radiocarbon time series: the 4-box model of Miyake *et al.* [25], the 11-box model of Güttler *et al.* [95] and the 22-box models of Büntgen *et al.* [23] and Brehm *et al.* [21].

We apply these to all published annual tree-ring data on all six known Miyake events, and infer posterior probability distributions for parametric and non-parametric models of the radiocarbon production rate over time, including the timing and duration, amplitude, and relation to the solar cycle. These posteriors determine a relationship to the solar cycle in 993 CE, 774 CE and 5410 BCE, though not for other events, and a range of total radiocarbon production delivering in a single pulse the equivalent of 1–4 years of average production.

2. Methods: the ticktack carbon box model framework

Carbon box models are widely used in literature from archaeology to geophysics. They span different levels of sophistication, from simple treatments of radiocarbon relative to carbon-12, through to full models of global geochemistry since the beginning of the Earth (e.g. [90]).

On the timescales that are relevant to single-year spikes of radiation, it is sufficient to consider only the dynamics of radiocarbon against a fixed background of equilibrium carbon flows. The overall properties of these models are specified by the reservoirs into which carbon is partitioned; the stable carbon content of each reservoir N_i^{12}, and the stable carbon flows specified in Gt/yr or in residence times (yr), F_{ij}^{12}; the reservoirs in which radiocarbon is produced by cosmic rays, and in what proportions, V_i; and the long-term average production rate of radiocarbon q_0.

The radiocarbon flux between reservoirs is then computed as

$$F_i^{14}j = \underbrace{\left(\frac{m_{14}}{m_{12}N_i^{12}}F_{ij}^{12} - \lambda\right)}_{\equiv M_{ij}} \cdot N_i^{14}, \tag{2.1}$$

where λ is the radioactive decay constant for ^{14}C and M_{ij} is a static transfer matrix. This allows us to simplify the CBM model for a radiocarbon state vector $\mathbf{y} \equiv [N_i^{14}]$ and vector of production coefficients $\mathbf{V} \equiv [V_i]$ as a linear, first-order ODE

$$\frac{\mathrm{d}\mathbf{y}}{\mathrm{d}t} = \mathbf{M}\mathbf{y} + Q(t)\mathbf{V}, \tag{2.2}$$

where the inhomogeneous term $Q(t)$ is the radiocarbon production rate. For constant $Q(t) = q_0$ this has a steady state solution $\mathbf{y}_0 = \mathbf{M}^{-1}q_0$. For computational reasons, we reparameterize the ODE to the form

$$\frac{\mathrm{d}(\mathbf{y} - \mathbf{y}_0)}{\mathrm{d}t} = (Q(t) - q_0)\mathbf{V}, \tag{2.3}$$

which can be efficiently solved with a range of adaptive step-size algorithms. The results also depend to some extent on assumptions made in matching model outputs to data, including the

[1]Named for the Malvina Reynolds song, *Little Boxes* (1962), in which little boxes are *all made out of ticky-tacky/And they all look just the same*.

Downloaded from https://royalsocietypublishing.org/ on 31 October 2022

growth seasons of trees and any short-term atmospheric dynamics; and in fitting these models to data, the algorithms used for optimization and inference.

We have developed an open-source, object-oriented Python package, `ticktack`, for specifying and running arbitrary CBMs. A user can input a series of `Box` and `Flow` objects with a numerical value for the reservoir or flow, units, and metadata (e.g. Northern or Southern Hemisphere, or the fraction of radiocarbon production in this box) and then compiles this to a `CarbonBoxModel` object; or they can load a pre-saved object. The user can then specify an equilibrium production condition—either directly a radiocarbon production rate, or it can find the production rate by gradient descent to reach a target ^{14}C quantity in a particular reservoir.

This `CarbonBoxModel` then has a method `run` which uses the JAX Dormand-Prince (DP5; [96]) algorithm as implemented in the Diffrax differential equation library [97] to solve the CBM ODE for a specified initial condition, production rate, and timesteps. Because this is implemented in Google JAX [92], this can be compiled, executed on GPUs, and is automatically differentiable, allowing for use in gradient descent optimization and Hamiltonian Monte Carlo [98].

We have followed the descriptions of four models used in the literature which are sufficiently well-described in terms of carbon reservoirs and flows to be emulated in `ticktack`, and which have been applied to Miyake event analysis: the 11-box Güttler *et al.* [95] and 4-box Miyake *et al.* [25], and 22-box Büntgen *et al.* [23], and Brehm *et al.* [21]. The 22-box models represent similar, but slightly different, partitions into two hemispheres of the global carbon cycle described in the 11-box model. All four models are available as default pre-saved models in `ticktack`.

`ticktack` is not a replacement for detailed models of the climate cycle, but rather for fast reconstruction of production from tree-ring data. Open source alternatives such as `pyhector` [99], Pymagicc [100] or the Simple Carbon Project (SCP-M; [91]) are geared towards climate modelling, for which our model is not sufficiently accurate, but are not fast enough to couple to Bayesian inference of radiocarbon production. SCP-M couples ocean dynamics to a carbon cycle model, with approximately 30 s runtime for 10 ky; we need to achieve $\ll 1$ s runtime for Markov Chain Monte Carlo (MCMC; [101]). We also do not aim to perform radiocarbon date calibration, for which there are several open-source libraries already available such as OxCal [102,103], BCal [104], MatCal [105] or ChronoModel [106].

(a) Parametric inference

We can use this model in forwards-mode to simulate time series of ^{14}C or Δ^{14}C ; and therefore also to solve the inverse problem of reconstructing radiocarbon production rates from data. We can load a tree-ring Δ^{14}C time series together with a CBM as a `SingleFitter` class object in `ticktack`, which has methods for parametric and non-parametric Bayesian inference of the production rate, or by direct inversion of the ODE. In this paper, we adopt a parametric model for production rate $Q(t)$, given steady state q_0, including three components

$$Q(t) = q_0 + A_\odot\, q_0 \sin\left(\frac{2\pi t}{11\,\mathrm{yr}} + \phi\right) + S(t, t_0, \Delta t) + m \cdot t, \tag{2.4}$$

where the solar cycle has an amplitude $A_\odot$ and phase ϕ; there is a long-term trend with gradient m. The Miyake event spike profile $S(t)$ is represented as a normalized super-Gaussian with start date t_0, duration Δt, and amplitude S_0:

$$S(t, t_0, \Delta t) \equiv \frac{S_0}{\Delta t} \exp\left(-\frac{t - (t_0 + \Delta t/2)}{1/1.93516\,\Delta t}^{16}\right). \tag{2.5}$$

The super-Gaussian form is chosen to approximate a top-hat function, but with differentiable sides more amenable to optimizers and ODE solvers. The numerical factor of 1.93516 is the integral of the unit super-Gaussian $\exp(-t^{16})$, and is used for normalization. The amplitudes of any of these coefficients can optionally be fixed at zero to disable each component of the production model.

Downloaded from https://royalsocietypublishing.org/ on 31 October 2022

This forwards model can be used with Bayesian tools to infer posterior probability distributions over the values of any of these parameters. We assume a Gaussian distribution for each Δ^{14}C sample with mean d_i and uncertainty σ_i, so that the log-likelihood of a parameter vector θ is

$$\log \mathcal{L}(\theta) = \sum_i \frac{d_i - Q(\theta)_i}{\sigma_i}, \tag{2.6}$$

and adopt uniform priors over phase and start date with reasonable limits, and log-uniform Jeffreys priors over all other parameters.

The `SingleFitter` class has methods for sampling from this posterior using MCMC as implemented in the affine-invariant ensemble sampler `emcee` [93,107], and nested sampling as implemented in JAXNS [94,108].

(b) Non-parametric inference

It is also possible to infer radiocarbon production rates per year directly from a Δ^{14}C time series, using either a direct inverse to the ODE, or by a forwards model with a flexible, high-dimensional parameterization.

The ODE can be solved exactly for a box i with non-zero production and measured data, such as from a tree-ring time series in the troposphere, by rearranging equation (2.2) to the form

$$Q = \frac{\dot{y}_i - (\mathbf{My})_i}{V_i}, \tag{2.7}$$

except that the flow term $\mathbf{My}$ depends on the radiocarbon state in *all* boxes simultaneously, so that it is also necessary to infer the missing components of the state vector.

To implement this inverse solver, Brehm *et al.* [21] take annual-cadence data, interpolate this to a continuous fine grid (for example to 12-month sampling), and in a finite-difference form of the CBM ODE to iteratively find the production rate at each timestep to reach the required tropospheric Δ^{14}C measurement at the next time step.

In `ticktack`, we implement an alternative non-iterative approach, by interpolating $y_i(t)$ linearly, and using JAX to differentiate this to obtain $\dot{y}_i(t)$. We can then obtain the full state history $\mathbf{y}(t)$ by solving the ODE with the production term from equation (2.7) and an initial steady state $\mathbf{y}_0$, and then use this completed state history to obtain $Q(t)$. This is exact for a finely sampled completed model, and in practice is a good approximation for data binned over a growth season if the time stamps are taken to be the middle of each growth season.

Because this inverse solver method relies on differentiation, when the signal-to-noise ratio is low it has the tendency to amplify noise on short timescales. In order to find a reconstruction that is more tolerant to noise, we want to use a Bayesian method as described above in §a, but choose a very flexible high-dimensional parameterization for $Q(t)$. Here, we will use a set of control points—a large but finite grid of points $\mathbf{q} \equiv [q(t_i)]$—as parameters, and use a Matérn–3/2 Gaussian process (GP; [109]) both to interpolate these to a smooth function of time, and also use the GP likelihood to penalize spurious short-timescale variations. We implement this GP calculation using the `tinygp` library [110], which is written in JAX and can therefore be compiled and differentiated along with the rest of `ticktack` .

While we do not attempt to do so here, it is also possible to solve this problem in the Fourier domain. The impulse response function of the carbon cycle to a pulse of radiation can be analytically determined as the matrix exponential

$$\mathbf{g}(t) = \mathbf{V} \exp(-\mathbf{M}\, t), \tag{2.8}$$

and an arbitrary time series in box i generated by the convolution $g_i(t) \star Q(t)$. The Fourier transform of $g_i(t)$ is a frequency response function that can be used as a linear filter in the Fourier domain, which Usoskin & Kromer [111] use as an alternative to iterative solution, but which is not implemented in `ticktack` in this study.

Downloaded from https://royalsocietypublishing.org/ on 31 October 2022

(c) Tree-ring data

We apply this code to an analysis of all publicly available Δ^{14}C data for the six events previously identified in the literature, gathering the COSMIC network data from many sites across both hemispheres for 774 CE and 993 CE from Büntgen *et al.* [23]; additional data, including early and late wood data, for 774 CE from Uusitalo *et al.* [112], and Danish oak over 993 CE from Fogtmann-Schulz *et al.* [64]; English oak over 993 CE from Rakowski *et al.* [113]; the discovery data for 7176 BCE and 5259 BCE from Brehm *et al.* [16]; earl tree-rings over 660 BCE from Park *et al.* [15], and early and late wood over 660 BCE from Sakurai *et al.* [24]; and data from the decades leading up to 5410 BCE from Miyake *et al.* [25]. We exclude the Japanese cedar from Miyake *et al.* [114], as it shows a delayed rise compared to the other 993 CE datasets, and for the purposes of the present work, we await a consensus on how to interpret this.

Before examining the modelled outputs in detail, some general observations should be made about the reliability and sensitivity of the underlying data. The apparent congruence of the sets of Δ^{14}C results, in both timing and amplitude, is especially remarkable given the data come from trees of various genera and species that grew in a wide range of different habitats. In reality, every individual tree is subject to its own specific environment and the biotic and abiotic disturbances that it poses, such as insect outbreaks, fungal diseases and climate anomalies [23]. As well as this, the physiology of each species determines the way it uses and/or reuses carbohydrates for growth-ring construction. This latter consideration lies at the core of an ongoing debate about whether whole rings or only late wood fractions should be analysed to achieve the highest quality data [64,115,116]. Furthermore, at per mille precisions intra-annual fluctuations in atmospheric radiocarbon concentrations also become significant, and in particular the coincidence of annual maxima and minima with the growing seasons of different species at different locations [117]. Finally, each laboratory employs its own celluose extraction technique, sometimes tailoring it to the individual species at hand. Such methodological differences have been shown to produce variations in data quality, even on samples of the same tree-rings [118].

Given all these complications, it is unsurprising that differences can be seen across the full suite of radiocarbon profiles. Nonetheless, there is one particular pattern which defies simple explanation, and may have some as yet unknown physical origin. Some 774 CE datasets exhibit an instantaneous uplift between 774 and 775 CE, while others show a more gradual rise over several years. The split between such sharp and prolonged rises in Δ^{14}C exists between different trees from similar environments, and even between trees of the same species from similar environments, as discussed in §4a. It is unclear whether this effect is astrophysical, environmental, to do with unknown tree-growth dynamics, or a systematic in the measurements.

3. Results

(a) Parametric fits

We used the workflow scheduling package Snakemake [119] to automatically execute and reproducibly log parametric fits as described in §2a to all six events, with the 774 CE event split into sharp and prolonged rise subsets. While we had the option to apply nested sampling, we used the affine-invariant ensemble MCMC sampler `emcee` exclusively in this section.

We infer the start data, duration, spike amplitude, phase and amplitude of the solar cycle, and a long-term linear trend, with the model initialized in steady state with the solar cycle.

Posterior ensembles of models overlaid on data, together with corresponding radiocarbon production histories, are displayed in figure 1, and they show overall excellent agreement with data. Corner plots of the parameter posteriors are available in electronic supplementary material.

Downloaded from https://royalsocietypublishing.org/ on 31 October 2022

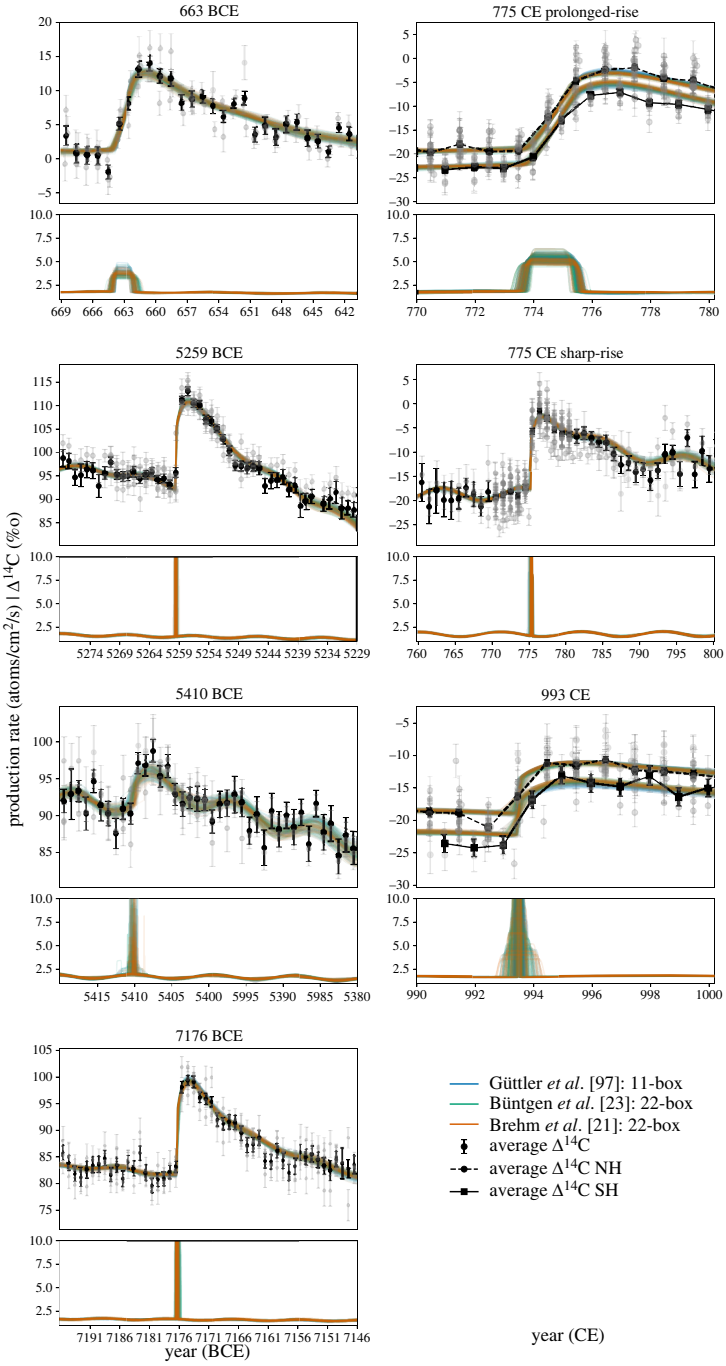

Figure 1. Results of MCMC fitting of a parametric Miyake event model to all six known events. Each is presented in a pair of panels. Top: the tree-ring data (individual trees in grey, mean in black) overlaid with colour-coded curves drawn at random from MCMC posterior samples for all three CBMs; they are in excellent agreement with one another and with the data. Bottom: radiocarbon production rate models drawn from the corresponding MCMC posterior samples, with the same colour bars. The 663 BCE event and a subset of the 774 CE event are consistent only with a production spike taking longer than a year. The 774 CE event is presented split into subsets of data showing a prolonged rise, and a sudden rise, which are incompatible in our models and analysed separately. (Online version in colour.)

Downloaded from https://royalsocietypublishing.org/ on 31 October 2022

(b) Non-parametric retrieval of production rates

In addition to the parametric fits displayed above, we applied both the GP and inverse solver non-parametric retrievals to the same datasets, and visualize the output similarly in figure 2. We again obtain a good fit to data, with the events occurring in the expected years, though now without the possibility of deconvolving structure at very short timescales. The GP and inverse solver produce results that are consistent with one another.

As an extension for future work, it is feasible to apply the inverse solver to the entire IntCal20 history, and use this as an initialization point for the reservoirs and production history of parametric fits at any particular point in time; this is a plausible strategy for making like-for-like comparison in absolute radiocarbon production between events occurring at times with different baseline production rates. We have elected not to do so here, to avoid introducing spurious transients in our sinusoidal production model, and without knowing a straightforward way to resolve this tension.

4. Discussion

We find excellent agreement between the three carbon box models emulating Güttler *et al.* [95], Brehm *et al.* [21], Büntgen *et al.* [23], with a closer agreement between the latter two models which are partitioned into northern and southern hemispheres. By contrast, as noted by Usoskin *et al.* [44], Miyake *et al.* [25] has a different normalization[2] and excludes the substantial carbon reservoir of the deep ocean, and we have excluded this from plots.

(a) Timing of 774 CE event

The 774 CE event occurs almost synchronously across the range of species and locations involved. However, there is some variation in the rate at which the increase is expressed. Broadly, there are two types of increases. About half of the datasets support a sharp rise—an anomalous jump in the data within 1 year—and the other half a more prolonged rise over 2–3 years. Furthermore, the latter group includes trees of the same species, in similar locations, measured at the same laboratories.

A similar late rise is found in Japanese cedar for the 993 CE event by Miyake *et al.* [114], who interpret this as being affected by global atmospheric circulation patterns in different latitudinal Radiocarbon Zones, and an oceanic versus continental distinction. By contrast, in the ensemble of tree rings over 774 CE, prolonged and sharp rises are seen across these categories: there are trees showing both phenomenologies from Zones 0-2, continental or oceanic regions, different growth speeds and altitudes. It is therefore not completely clear what is the cause of this split in 774 CE phenomenologies. In future work, there may be insights from global circulation models of the atmosphere, together with improved precision and sample size for tree-ring data over these events.

(b) Miyake event amplitude and duration

In order to investigate the astrophysical origin of the Miyake events, it is of primary importance to determine their fundamental parameters—especially their size and duration. Posterior distributions of spike production relative to the steady state are displayed in figure 3.

Because we work with Δ^{14}C rather than absolute ^{14}C , we report the integrated spike radiocarbon production in units of equivalent years of steady state production: i.e. a spike amplitude of 1 in these units indicates a total production of 1 q_0 yr. In these units, the smallest event is 5410 BCE, with a total production a shy of 1 q_0 yr, followed by 993 CE at around 2 q_0 yr

[2]In Miyake [120], it is explained that an equilibrium production rate is assumed over a $\pi R_\oplus^2$ Earth cross-sectional area, as opposed to a $4\pi R_\oplus^2$ isotropic area, and this leads to a different assumption about equilibrium production rates.

Downloaded from https://royalsocietypublishing.org/ on 31 October 2022

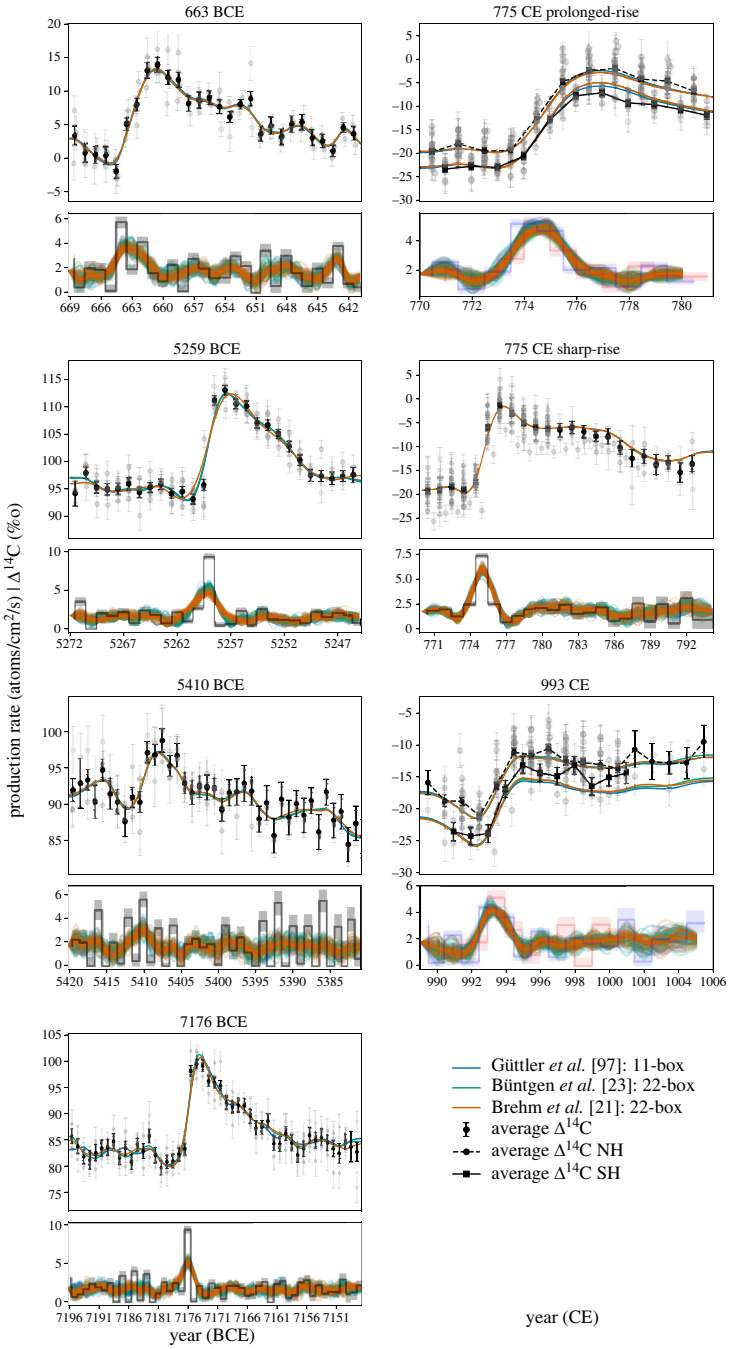

Figure 2. Results of MCMC fitting of a non-parametric control-points radiocarbon production rate model to all six known events. Each is presented in a pair of panels. Top: the tree-ring data (individual trees in grey, mean in black) overlaid with colour-coded curves drawn at random from MCMC posterior samples for all three CBMs. Bottom: radiocarbon production rate models drawn from the corresponding MCMC posterior samples, with the same colour bars; durations greater than a year are a necessary feature of the control points method and not strong evidence of long duration events. The 774 CE event is presented split into subsets of data showing separately a prolonged rise, and a sudden rise. (Online version in colour.)

Downloaded from https://royalsocietypublishing.org/ on 31 October 2022

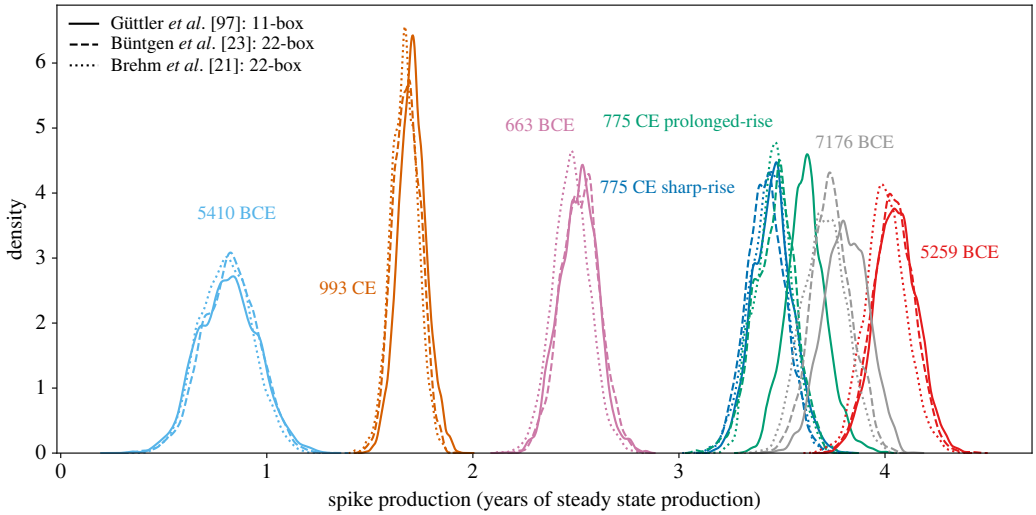

Figure 3. Marginal posterior probability distributions for the total radiocarbon production inferred for all six known Miyake events. This is calculated as the area under a spike, irrespective of its duration, minus the steady state, in units of equivalent years of steady-state production. Different events are denoted by colour, and different CBMs by solid [95], dashed [23] and dotted [21] lines. The datasets showing a short or prolonged rise for 774 CE are shown separately. (Online version in colour.)

and 663 BCE at around 2.5 q_0 yr. The 775 CE and 7176 BCE events are in excess of 3 q_0 yr, and the largest of all is 5259 BCE at around 4 q_0 yr.

We are intentionally wary of attempting a conversion of this to absolute kg^{14}C, which would bring in the more-uncertain q_0 at the time of each event, or of correcting this for the geomagnetic field, as this requires assumptions about the origin and spectrum of particles. Nevertheless, it is interesting that in these units the spike amplitudes are all of order unity—as might be expected from a change of order unity to heliospheric shielding of Galactic cosmic rays, for a duration of order 1 year.

The marginal posterior distributions for duration are displayed in figure 4, showing that while 7176 BCE, 5259 BCE, and a subset of 775 CE data are consistent with durations of <1 yr, the duration of 5410 BCE is very poorly constrained, a subset of 775 CE data indicate a duration of around 2 years (for these trees, 100% of posterior samples have durations >1 yr, and approx. 15% > 2 yr), and 663 BCE has a duration of 2–3 years. There is a somewhat extended tail in the posterior for 993 CE, with 20% of samples showing durations >6 months, although only approx. 4% > 1 yr. These are all covariant with start date, as seen in the corner plots in the electronic supplementary material: an early start and a long duration, or a late start and a brief duration, are both compatible with the data due to the 1-year sampling limitation. This is marginal evidence against a model of the Miyake events arising from a single short impulse; this can only be confirmed with multi-isotopic data, such as from ice cores where finer time sampling is achievable, and from a better understanding of the systematics induced by growth seasons and geography in tree-ring time series.

(c) Relation to the solar cycle

High solar magnetic field strength gives rise to low ^{14}C production, because the solar magnetic field shields the Earth from galactic cosmic rays. Therefore, we can define solar maxima to be the minima of the 11-year sinusoidal component of ^{14}C production. Our Bayesian posteriors for solar cycle phase ϕ show no consistent pattern. Moreover, our histograms of the event timing, relative to solar cycle in figure 5, also show no obvious connection. We find that 5410 BCE occurs at or shortly before solar minimum, 5259 CE a couple of years after, while 774 CE occurs 2 years

Downloaded from https://royalsocietypublishing.org/ on 31 October 2022

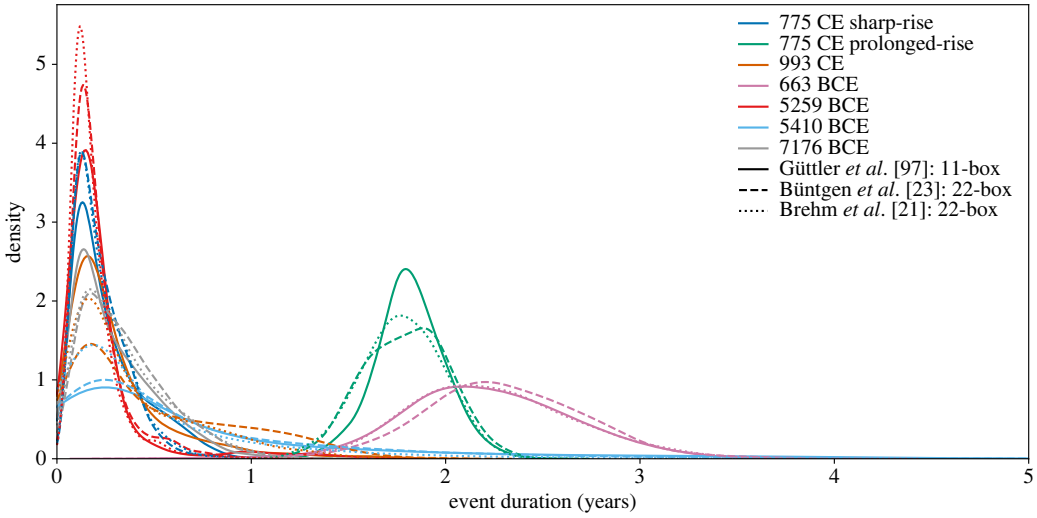

Figure 4. Marginal posterior probability distributions for the duration of all six known Miyake events. Different events are denoted by colour, and different CBMs by solid [95], dashed [23] and dotted [21] lines. The datasets showing a short or prolonged rise for 774 CE are shown separately. (Online version in colour.)

before maximum. The 993 CE event is more difficult to resolve. The increase seems to occur at a solar minimum in some runs, but the analysis is currently lacking in sufficient data for any firm conclusions. As a result, this event is excluded from figure 5 but further data will undoubtedly improve on this outcomes. With regard to the 7176 BCE event, Paleari *et al.* [121] believe the ^{10}Be evidence supports its occurrence at a solar minimum. In contrast to that study as well as Scifo *et al.* [65] and Miyake *et al.* [17], our findings show no clear relationship between the appearance of one of these events and the phase of the solar cycle, though with only three examples so far we cannot statistically reject any dependence.

(d) Dependence on latitude

In the case of an extreme solar event, a greater particle flux and therefore radiocarbon production is expected near the poles than the equator. Both Büntgen *et al.* [23] and Uusitalo *et al.* [112] claim that the amplitude of the events as recorded by northern hemisphere tree rings is increased closer to the North Pole. In order to examine this possible trend, we fit every tree individually for spike amplitude, timing and duration, while holding parameters of the solar cycle constant at the ensemble mean. We then used `emcee` to fit a line and infer parameter uncertainties, including an additional term for underestimated error bars. Our outputs provide no convincing evidence for this effect. With our larger sample of trees, we find the slope to be $(9.8 \pm 8.8) \times 10^{-3}$ steady-state years per degree north, with a 13% probability the slope is less than zero. In the main, this possible latitudinal trend largely goes away because of the scatter observed in the array of data available from mid-latitudes, see figure 6.

5. Conclusion

In this work, we have combined fast CBM models with modern Bayesian inference tools, and applied them to the ensemble of existing data on Miyake events. From the posterior parameter distributions we infer, we find no clear relation in timing to the solar cycle, or in amplitude to latitude as has previously been claimed; and we find some evidence of extended duration not only in 663 BCE, but also in 775 and to some extent in 993 CE. This can be interpreted either as a real astrophysical non-zero duration, or as a noise floor on time resolution owing to the

Downloaded from https://royalsocietypublishing.org/ on 31 October 2022

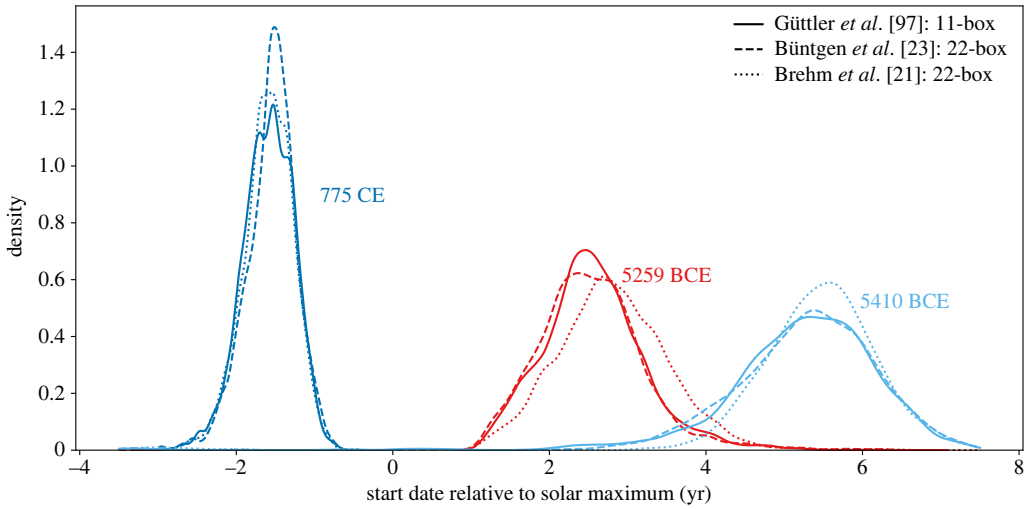

Figure 5. Marginal posterior probability distributions for the timing relative to the Solar Cycle of three Miyake events for which significant solar cycles are detected: 774 CE, 5259 BCE and 5410 BCE . Assuming the minimum of solar activity corresponds to a maximum of radiocarbon production rate, we find that 5259 BCE and 5410 BCE occur at or shortly before solar minima, while 774 CE occurs 2 years before maximum. Different events are denoted by colour, and different CBMs by solid [95], dashed [23] and dotted [21] lines. (Online version in colour.)

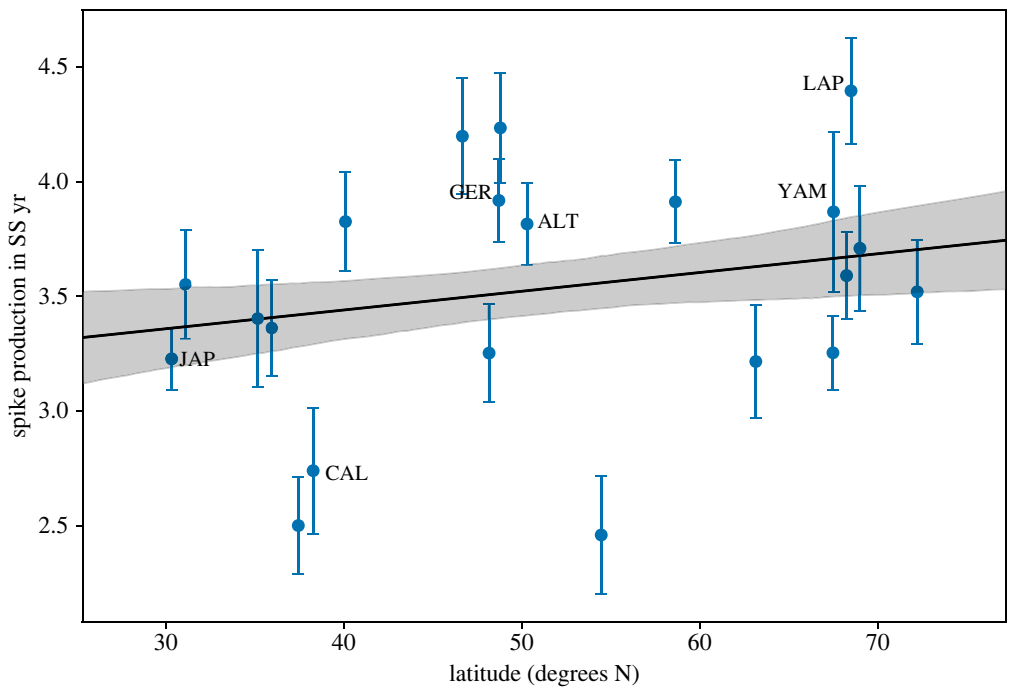

Figure 6. Scatter plot with 1 σ errorbars of 774 CE spike amplitude recorded in individual trees as a function of latitude, overlaid with best-fit line and shaded between 16,84 percentiles of posterior draws. While a trend with latitude has been used to support a solar origin [112], with our larger sample of trees we find the slope to be $(9.8 \pm 8.8) \times 10^{-3}$ steady-state years per degree north. (Online version in colour.)

Downloaded from https://royalsocietypublishing.org/ on 31 October 2022

growth conditions and biology of the trees, model uncertainties in the preindustrial carbon cycle, and/or to atmospheric dynamics not captured by the carbon box model. In order to resolve this question, in future work, we will want to obtain larger samples of high-precision, annual-cadence tree-rings over these well-studied events; multiradionuclide time series, including subannually resolved ^{36}Cl and ^{10}Be from ice-cores; and systematically compare CBM implementations to global circulation models that accurately capture the latitudinal and stratosphere–troposphere exchange of radiocarbon.

If the measured extended durations are reproduced, and are owing to biological or atmospheric processes, these will impose a precision floor of order approximately 1 year on radiocarbon dating with these Miyake events (such as done for L'Anse aux Meadows by [32]). On the other hand, if the prolonged radionuclide production has an astrophysical origin, this will be hard to reconcile with an impulsive production model of one large energetic particle burst, whether of solar energetic particles or from a stellar remnant. In light of this, we recommend that it is important to obtain improved multiradionuclide data across the 5480 BCE decade-long radiocarbon rise, and the 3-year 663 BCE event, as they may form a continuum in duration with the other shorter radiation bursts.

There is very significant scope to improve open-source software for carbon isotope analysis. `ticktack` can emulate the parameters of a range of existing CBMs: future work would also systematically compare the different CBM parameters to one another and to data in a range of contexts, including varying the stratosphere-to-troposphere production coefficients. `ticktack` is also extensible to connect to other inference tools: because the solver is implemented in JAX, it would be straightforward to implmement a Hamiltonian Monte Carlo sampler for very large or complex models using the probabilistic programming language `numpyro` [122], including a more sophisticated treatment of priors. A project beyond `ticktack` would solve for multiple isotopes, and include effects of atmospheric dynamics and geochemistry. In the long term, it would be worth applying MCMC to more complex models for a variety of applications, including inferring the parameters of the preindustrial carbon cycle directly from radiocarbon data, or inferring growth seasons and timing of different trees. We expect that there will be many applications for fast, differentiable carbon cycle models connected to modern Bayesian frameworks across geo- and astro-physics.

Data accessibility. In the interests of open science, we have made the `ticktack` code available under an MIT open source license at github.com/sharmallama/ticktack, with documentation provided at sharmallama.github.io/ticktack. The Snakemake workflow used to analyse the data is available at github.com/qingyuanzhang3/radiocarbon_workflow. We encourage and welcome other scientists to replicate, apply and extend our work. The data are provided in electronic supplementary material [123].

Authors' contributions. Q.Z.: data curation, formal analysis, investigation, methodology, software, visualization, writing—review and editing; U.S.: data curation, investigation, methodology, software, visualization; J.A.D.: methodology, software, writing—review and editing; A.S.: methodology, resources, writing—review and editing; M.K.: investigation, resources, writing—review and editing; U.B.: investigation, methodology, resources, writing—review and editing; M.J.O.: conceptualization, investigation, methodology, writing—review and editing; M.W.D.: conceptualization, funding acquisition, investigation, methodology, project administration, resources, supervision, writing—review and editing; B.J.S.P.: conceptualization, investigation, methodology, project administration, resources, software, supervision, writing—original draft, writing—review and editing.

All authors gave final approval for publication and agreed to be held accountable for the work performed therein.

Conflict of interest declaration. The authors declare no competing interests.

Funding. This research was supported by the UQ Winter and Summer Research Scholarships, and the inaugural UQ Fellowship of the Big Questions Institute.

Acknowledgements. We would like to thank Andrew Smith, David Fink, Quan Hua and the anonymous referees for their helpful comments on this manuscript. We would like to acknowledge the traditional owners of the land on which the University of Queensland is situated, the Turrbal and Jagera people. We pay respects to their Ancestors and descendants, who continue cultural and spiritual connections to Country. This research made use of the IPYTHON package [124]; Snakemake [119]; NUMPY [125]; MATPLOTLIB [126]; SCIPY [127];

Downloaded from https://royalsocietypublishing.org/ on 31 October 2022

Google JAX [92]; `ChainConsumer` [128]; `emcee` [93]; JAXNS [94]; and we emulate the models of Güttler *et al.* [95], Miyake *et al.* [25], Büntgen *et al.* [23] and Brehm *et al.* [21].

References

1. Kern EM. 2020 Archaeology enters the 'atomic age': a short history of radiocarbon, 1946–1960. *Br. J. History Sci.* **53**, 207–227. (doi:10.1017/S0007087420000011)
2. Hajdas I, Ascough P, Garnett MH, Fallon SJ, Pearson CL, Quarta G, Spalding KL, Yamaguchi H, Yoneda M. 2021 Radiocarbon dating. *Nat. Rev. Methods Primers* **1**, 1–26. (doi:10.1038/s43586-021-00058-7)
3. Libby WF, Anderson EC, Arnold JR. 1949 Age determination by radiocarbon content: world-wide assay of natural radiocarbon. *Science* **109**, 227–228. (doi:10.1126/science.109.2827.227)
4. Stuiver M, Braziunas TF. 1993 Sun, ocean, climate and atmospheric $^{14}CO_2$: an evaluation of causal and spectral relationships. *Holocene* **3**, 289–305. (doi:10.1177/095968369300300401)
5. Heaton TJ, Bard E, Bronk Ramsey C, Butzin M, Köhler P, Muscheler R, Reimer PJ, Wacker L. 2021 Radiocarbon: a key tracer for studying Earth's dynamo, climate system, carbon cycle, and Sun. *Science* **374**, 7096eabddoi:10.1126/science.abd7096)
6. de Vries H. 1958 Variation in concentration of radiocarbon with time and location on earth. *Proc. KNAW (Royal Dutch Academy of Sciences)* **B61**, 94–102.
7. Suess HE. 1970 Bristle-cone pine calibration of the radiocarbon time-scale, 5200 BC To the present. In *Radiocarbon variations and absolute chronology, Proc. of XIIth Nobel Symp.*, Uppsala, Sweden, pp. 303–308. New York, NY: John Wiley & Sons.
8. Reimer PJ *et al.* 2013 IntCal13 and Marine13 radiocarbon age calibration Curves 0–50 000 years cal BP. *Radiocarbon* **55**, 1869–1887. (doi:10.2458/azu_js_rc.55.16947)
9. Reimer PJ *et al.* 2020 The IntCal20 northern hemisphere radiocarbon age calibration curve (0–55 cal kBP). *Radiocarbon* **62**, 725–757. (doi:10.1017/rdc.2020.41)
10. Heaton TJ, Blaauw M, Blackwell PG, Ramsey CB, Reimer PJ, Scott EM. 2020 The IntCal20 approach to radiocarbon calibration curve construction: a new methodology using Bayesian splines and errors-in-variables. *Radiocarbon* **62**, 821–863. (doi:10.1017/rdc.2020.46)
11. Hogg AG *et al.* 2020 SHCal20 Southern Hemisphere Calibration, 0–55 000 Years cal BP. *Radiocarbon* **62**, 759–778. (doi:10.1017/rdc.2020.59)
12. Güttler D, Wacker L, Kromer B, Friedrich M, Synal HA. 2013 Evidence of 11-year solar cycles in tree rings from 1010 to 1110 AD–progress on high precision AMS measurements. *Nucl. Instrum. Methods Phys. Res., Sect. B* **294**, 459–463. (doi:10.1016/j.nimb.2012.08.046)
13. Miyake F, Nagaya K, Masuda K, Nakamura T. 2012 A signature of cosmic-ray increase in AD 774-775 from tree rings in Japan. *Nature* **486**, 240–242. (doi:10.1038/nature11123)
14. Miyake F, Masuda K, Nakamura T. 2013 Another rapid event in the carbon-14 content of tree rings. *Nat. Commun.* **4**, 1748. (doi:10.1038/ncomms2783)
15. Park J, Southon J, Fahrni S, Creasman PP, Mewaldt R. 2017 Relationship between solar activity and $\Delta^{14}C$ peaks in AD 775, AD 994, and 660 BC. *Radiocarbon* **59**, 1147–1156. (doi:10.1017/RDC.2017.59)
16. Brehm N *et al.* 2022 Tree-rings reveal two strong solar proton events in 7176 and 5259 BCE. *Nat. Commun.* **13**, 1–8. (doi:10.1038/s41467-022-28804-9)
17. Miyake F *et al.* 2021 A single-year cosmic ray event at 5410 BCE registered in ^{14}C of tree rings. *Geophys. Res. Lett.* **48**, e2021GL093419.
18. Jull AJT *et al.* 2018 More rapid ^{14}C excursions in the tree-ring record: a record of different kind of solar activity at about 800 BC? *Radiocarbon* **60**, 1237–1248. (doi:10.1017/RDC.2018.53)
19. Wang FY, Yu H, Zou YC, Dai ZG, Cheng KS. 2017 A rapid cosmic-ray increase in BC 3372–3371 from ancient buried tree rings in China. *Nat. Commun.* **8**, 1–5. (doi:10.1038/s41467-017-01698-8)
20. Jull AJT *et al.* 2021 Rapid ^{14}C excursion at 3372-3371 BCE not observed at two different locations. *Nat. Commun.* **12**, 1–3. (doi:10.1038/s41467-020-20695-y)
21. Brehm N *et al.* 2021 Eleven-year solar cycles over the last millennium revealed by radiocarbon in tree rings. *Nat. Geosci.* **14**, 10–15. (doi:10.1038/s41561-020-00674-0)
22. Miyahara H, Tokanai F, Moriya T, Takeyama M, Sakurai H, Ohyama M, Horiuchi K, Hotta H. 2022 Recurrent large-scale solar proton events before the onset of the wolf grand solar minimum. *Geophys. Res. Lett.* **49**, e2021GL097201. (doi:10.1029/2021gl097201)

Downloaded from https://royalsocietypublishing.org/ on 31 October 2022

23. Büntgen U *et al.* 2018 Tree rings reveal globally coherent signature of cosmogenic radiocarbon events in 774 and 993 CE. *Nat. Commun.* **9**, 3605.
24. Sakurai H *et al.* 2020 Prolonged production of ^{14}C during the 660 BCE solar proton event from Japanese tree rings. *Sci. Rep.* **10**, 660. (doi:10.1038/s41598-019-57273-2)
25. Miyake F *et al.* 2017 Large ^{14}C excursion in 5480 BC indicates an abnormal sun in the mid-Holocene. *Proc. Natl Acad. Sci. USA* **114**, 881–884. (doi:10.1073/pnas.1613144114)
26. Kanzawa K *et al.* 2021 High-Resolution ^{10}Be and ^{36}Cl Data from the Antarctic Dome Fuji ice core (100 years around 5480 BCE): an unusual grand solar minimum occurrence? *J. Geophys. Res. (Space Physics)* **126**, e29378.
27. Dee MW, Pope BJS. 2016 Anchoring historical sequences using a new source of astro-chronological tie-points. *Proc. R. Soc. A* **472**, 20160263. (doi:10.1098/rspa.2016.0263)
28. Oppenheimer C *et al.* 2017 Multi-proxy dating the 'Millennium Eruption' of Changbaishan to late 946 CE. *Quat. Sci. Rev.* **158**, 164–171. (doi:10.1016/j.quascirev.2016.12.024)
29. Hakozaki M, Miyake F, Nakamura T, Kimura K, Masuda K, Okuno M. 2018 Verification of the annual dating of the 10th Century Baitoushan Volcano eruption based on an AD 774–775 radiocarbon spike. *Radiocarbon* **60**, 261–268.
30. Kuitems M, Panin A, Scifo A, Arzhantseva I, Kononov Y, Doeve P, Neocleous A, Dee M. 2020 Radiocarbon-based approach capable of subannual precision resolves the origins of the site of Por-Bajin. *Proc. Natl Acad. Sci. USA* **117**, 14038–14041.
31. Philippsen B, Feveile C, Olsen J, Sindbæk SM. 2021 Single-year radiocarbon dating anchors Viking Age trade cycles in time. *Nature* **601**, 392–396. (doi:10.1038/s41586-021-04240-5)
32. Kuitems M *et al.* 2021 Evidence for European presence in the Americas in AD 1021. *Nature* **601**, 388–391. (doi:10.1038/s41586-021-03972-8)
33. Cliver EW, Schrijver CJ, Shibata K, Usoskin IG. 2022 Extreme solar events. *Living Rev. Sol. Phys.* **19**, 2. (doi:10.1007/s41116-022-00033-8)
34. Hambaryan VV, Neuhäuser R. 2013 A Galactic short gamma-ray burst as cause for the ^{14}C peak in AD 774/5. *Mon. Not. R. Astron. Soc.* **430**, 32–36. (doi:10.1093/mnras/sts378)
35. Pavlov AK, Blinov AV, Konstantinov AN, Ostryakov VM, Vasilyev GI, Vdovina MA, Volkov PA. 2013 AD 775 pulse of cosmogenic radionuclides production as imprint of a Galactic gamma-ray burst. *Mon. Not. R. Astron. Soc.* **435**, 2878–2884.
36. Dee M, Pope B, Miles D, Manning S, Miyake F. 2016 Supernovae and single-year anomalies in the atmospheric radiocarbon record. *Radiocarbon* **59**, 293–302. (doi:10.1017/rdc.2016.50)
37. Terrasi F *et al.* 2020 Can the ^{14}C production in 1055 CE be affected by SN1054? *Radiocarbon* **62**, 1403–1418. (doi:10.1017/rdc.2020.58)
38. Wang FY, Li X, Chernyshov DO, Hui CY, Zhang GQ, Cheng KS. 2019 Consequences of energetic magnetar-like outbursts of nearby neutron stars: ^{14}C events and the cosmic electron spectrum. *Astrophys. J.* **887**, 202. (doi:10.3847/1538-4357/ab55db)
39. Pavlov AK, Frolov DA, Konstantinov AN, Koudriavtsev IV, Ogurtsov MG, Ostryakov VM, Vasilyev GI. 2019 On the radiocarbon increase around 5480 BC as a result of the Solar system encounter with interstellar cloud. *Mon. Not. R. Astron. Soc.* **485**, 4441–4445.
40. Pavlov AK, Blinov AV, Frolov DA, Konstantinov AN, Koudriavtsev IV, Ogurtsov MG, Ostryakov VM, Vasilyev GI. 2019 Isotopic imprint of the Solar system encounter with interstellar gas cloud around 660 BC (2610 BP). *J. Phys. Conf. Ser.* **1400**, 022034.
41. Liu Y *et al.* 2014 Mysterious abrupt carbon-14 increase in coral contributed by a comet. *Sci. Rep.* **4**, 1–4. (doi:10.1038/srep03728)
42. Usoskin IG, Kovaltsov GA. 2015 The carbon-14 spike in the 8th century was not caused by a cometary impact on Earth. *Icarus* **260**, 475–476. (doi:10.1016/j.icarus.2014.06.009)
43. Melott AL, Thomas BC. 2012 Causes of an AD 774-775 ^{14}C increase. *Nature* **491**, E1. (doi:10.1038/nature11695)
44. Usoskin IG, Kromer B, Ludlow F, Beer J, Friedrich M, Kovaltsov GA, Solanki SK, Wacker L. 2013 The AD775 cosmic event revisited: the Sun is to blame. *Astron. Astrophys.* **552**, L3. (doi:10.1051/0004-6361/201321080)
45. Neuhäuser R, Neuhäuser DL. 2015 Variations of ^{14}C around AD 775 and AD 1795 - due to solar activity. *Astron. Nachr.* **336**, 930. (doi:10.1002/asna.201512208)
46. Miyake F, Suzuki A, Masuda K, Horiuchi K, Motoyama H, Matsuzaki H, Motizuki Y, Takahashi K, Nakai Y. 2015 Cosmic ray event of A.D 774-775 shown in quasi-annual ^{10}Be

Downloaded from https://royalsocietypublishing.org/ on 31 October 2022

data from the Antarctic Dome Fuji ice core. *Geophys. Res. Lett.* **42**, 84–89. (doi:10.1002/2014GL062218)

47. Mekhaldi F *et al.* 2015 Multiradionuclide evidence for the solar origin of the cosmic-ray events of AD 774/5 and 993/4. *Nat. Commun.* **6**, 8611.
48. Webber WR, Higbie PR, McCracken KG. 2007 Production of the cosmogenic isotopes ^{3}H, ^{7}Be, ^{10}Be, and ^{36}Cl in the Earth's atmosphere by solar and galactic cosmic rays. *J. Geophys. Res.: Space Phys.* **112**, 1–7. (doi:10.1029/2007ja012499)
49. Mekhaldi F, Adolphi F, Herbst K, Muscheler R. 2021 The signal of solar storms embedded in cosmogenic radionuclides: detectability and uncertainties. *J. Geophys. Res. (Space Physics)* **126**, e29351.
50. Borucki WJ *et al.* 2010 Kepler planet-detection mission: introduction and first results. *Science* **327**, 977.
51. Okamoto S, Notsu Y, Maehara H, Namekata K, Honda S, Ikuta K, Nogami D, Shibata K. 2021 Statistical properties of superflares on solar-type stars: results using all of the kepler primary mission data. *Astrophys. J.* **906**, 72.
52. Nogami D, Notsu Y, Honda S, Maehara H, Notsu S, Shibayama T, Shibata K. 2014 Two sun-like superflare stars rotating as slow as the Sun∗. *Publicationse Astron. Soc. Jpn* **66**, L4.
53. Notsu Y *et al.* 2019 Do kepler superflare stars really include slowly rotating sun-like stars?–Results using APO 3.5 m telescope spectroscopic observations and Gaia-DR2 data. *Astrophys. J.* **876**, 58.
54. Hudson HS. 2021 Carrington events. *Annu. Rev. Astron. Astrophys.* **59**, 445–477.
55. Neuhäuser R, Hambaryan VV. 2014 A solar super-flare as cause for the ^{14}C variation in AD 774/5? *Astron. Nachr.* **335**, 949.
56. Usoskin IG, Koldobskiy SA, Kovaltsov GA, Rozanov EV, Sukhodolov TV, Mishev AL, Mironova IA. 2020 Revisited reference solar proton event of 23 February 1956: assessment of the cosmogenic-isotope method sensitivity to extreme solar events. *J. Geophys. Res. (Space Physics)* **125**, e27921.
57. Cliver EW, Hayakawa H, Love JJ, Neidig DF. 2020 On the size of the flare associated with the solar proton event in 774 AD. *Astrophys. J.* **903**, 41. (doi:10.3847/1538-4357/abad93)
58. Mekhaldi F *et al.* 2017 No coincident nitrate enhancement events in polar ice cores following the largest known solar storms. *J. Geophys. Res. (Atmospheres)* **122**, 11 900–11 913.
59. Sukhodolov T *et al.* 2017 Atmospheric impacts of the strongest known solar particle storm of 775 AD. *Sci. Rep.* **7**, 1–9. (doi:10.1038/srep45257)
60. Jackman JAG, Shkolnik E, Loyd ROP. 2021 Stellar flares from blended and neighbouring stars in Kepler short cadence observations. *Mon. Not. R. Astron. Soc.* **502**, 2033–2042.
61. Owens MJ, Lockwood M, Barnard LA, Scott CJ, Haines C, Macneil A. 2021 Extreme space-weather events and the solar cycle. *Sol. Phys.* **296**, 1–9. (doi:10.1007/s11207-021-01831-3)
62. Barnard L, McCracken KG, Owens MJ, Lockwood M. 2018 What can the annual ^{10}Be solar activity reconstructions tell us about historic space weather? *J. Space Weather Space Clim.* **8**, A23.
63. Miyake F, Masuda K, Nakamura T. 2013 Lengths of Schwabe cycles in the seventh and eighth centuries indicated by precise measurement of carbon-14 content in tree rings. *J. Geophys. Res. (Space Physics)* **118**, 7483–7487.
64. Fogtmann-Schulz A, Østbø SM, Nielsen SGB, Olsen J, Karoff C, Knudsen MF. 2017 Cosmic ray event in 994 C.E. recorded in radiocarbon from Danish oak. *Geophys. Res. Lett.* **44**, 8621–8628. (doi:10.1002/2017gl074208)
65. Scifo A *et al.* 2019 Radiocarbon production events and their potential relationship with the Schwabe cycle. *Sci. Rep.* **9**, 17056.
66. Stephenson FR. 2015 Astronomical evidence relating to the observed ^{14}C increases in A.D. 774-5 and 993-4 as determined from tree rings. *Adv. Space Res.* **55**, 1537–1545.
67. Allen J. 2012 Clue to an ancient cosmic-ray event? *Nature* **486**, 473–473. (doi:10.1038/486473e)
68. Neuhäuser DL, Neuhäuser R. 2015 'A red cross appeared in the sky' and other celestial signs: presumable European aurorae in the mid AD 770s were halo displays. *Astron. Nachr.* **336**, 913.
69. Hayakawa H, Stephenson FR, Uchikawa Y, Ebihara Y, Scott CJ, Wild MN, Wilkinson J, Willis DM. 2019 The celestial sign in the anglo-saxon chronicle in the 770s: insights on contemporary solar activity. *Sol. Phys.* **294**, 42.
70. Zhou D, Wang C, Zhang B, Zhang S, Zhou P, Sun Y, Liang J, Zhu G, Wu J. 2014 Super solar particle event around AD775 was found. *Chin. Sci. Bull.* **59**, 2736–2742. (doi:10.1007/s11434-014-0345-z)

Downloaded from https://royalsocietypublishing.org/ on 31 October 2022

71. Baum AC, Wright JT, Luhn JK, Isaacson H. 2022 Five decades of chromospheric activity in 59 sun-like stars and new maunder minimum candidate HD 166620. *Astron. J.* **163**, 183. (doi:10.3847/1538-3881/ac5683)
72. Luhn JK, Wright JT, Henry GW, Saar SH, Baum AC. 2022 HD 166620: portrait of a star entering a grand magnetic minimum. (http://arxiv.org/abs/2207.00612)
73. Barnes SA. 2003 On the rotational evolution of solar- and late-type stars, its magnetic origins, and the possibility of stellar gyrochronology. *Astrophys. J.* **586**, 464–479.
74. Angus R, Aigrain S, Foreman-Mackey D, McQuillan A. 2015 Calibrating gyrochronology using Kepler asteroseismic targets. *Mon. Not. R. Astron. Soc.* **450**, 1787–1798.
75. Van Saders JL, Ceillier T, Metcalfe TS, Aguirre VS, Pinsonneault MH, García RA, Mathur S, Davies GR. 2016 Weakened magnetic braking as the origin of anomalously rapid rotation in old field stars. *Nature* **529**, 181–184.
76. Hall OJ *et al.* 2021 Weakened magnetic braking supported by asteroseismic rotation rates of Kepler dwarfs. *Nat. Astron.* **5**, 707–714.
77. Metcalfe TS *et al.* 2022 The origin of weakened magnetic braking in old solar analogs. *Astrophys. J. Lett.* **933**, L17.
78. Böhm-Vitense E. 2007 Chromospheric activity in G and K main-sequence stars, and what it tells us about stellar dynamos. *Astrophys. J. Lett.* **657**, 486–493.
79. Metcalfe TS, Egeland R, van Saders J. 2016 Stellar evidence that the solar dynamo may be in transition. *Astrophys. J. Lett.* **826**, L2.
80. Reinhold T, Shapiro AI, Solanki SK, Montet BT, Krivova NA, Cameron RH, Amazo-Gómez EM. 2020 The Sun is less active than other solar-like stars. *Science* **368**, 518–521.
81. Jyothi SA. 2021 Solar superstorms. In *Proceedings of the 2021 ACM SIGCOMM 2021 Conf.* ACM.
82. Fujita M, Sato T, Saito S, Yamashiki Y. 2021 Probabilistic risk assessment of solar particle events considering the cost of countermeasures to reduce the aviation radiation dose. *Sci. Rep.* **11**, 17091.
83. Hubert G, Aubry S. 2021 Study of the impact of past extreme solar events on the modern air traffic. *Space Weather* **19**, e02665.
84. Sato T, Yasuda H, Niita K, Endo A, Sihver L. 2008 Development of PARMA: PHITS-based analytical radiation model in the atmosphere. *Radiat. Res.* **170**, 244–259. (doi:10.1667/rr1094.1)
85. Craig H. 1957 The natural distribution of radiocarbon and the exchange time of carbon dioxide between atmosphere and sea. *Tellus* **9**, 1–7.
86. Oeschger H, Siegenthaler U, Schotterer U, Gugelmann A. 1975 A box diffusion model to study the carbon dioxide exchange in nature. *Tellus* **27**, 168–192.
87. Siegenthaler U, Heimann M, Oeschger H. 1980 ^{14}C variations caused by changes in the global carbon cycle. *Radiocarbon* **22**, 177–191.
88. Nakamura T, Nakai N, Ohishi S. 1987 Applications of environmental ^{14}C measured by AMS as a carbon tracer. *Nucl. Instrum. Methods Phys. Res., Sect. B* **29**, 355–360.
89. Dorman LI. 2004 *Cosmic rays in the Earth's atmosphere and underground*. Dordrecht, Netherlands: Springer Science & Business Media.
90. Krissansen-Totton J, Catling DC. 2017 Constraining climate sensitivity and continental versus seafloor weathering using an inverse geological carbon cycle model. *Nat. Commun.* **8**, 1–5. (doi:10.1038/ncomms15423)
91. O'Neill CM, Hogg AM, Ellwood MJ, Eggins SM, Opdyke BN. 2019 The [simple carbon project] model v1.0. *Geosci. Model Dev.* **12**, 1541–1572. (doi:10.5194/gmd-12-1541-2019)
92. Bradbury J *et al.* 2018 JAX: composable transformations of Python+NumPy programs. See http://github.com/google/jax.
93. Foreman-Mackey D, Hogg DW, Lang D, Goodman J. 2013 emcee: the MCMC Hammer. *Publ. Astron. Soc. Pac.* **125**, 306.
94. Albert JG. 2020 JAXNS: a high-performance nested sampling package based on JAX. (http://arxiv.org/abs/2012.15286)
95. Güttler D *et al.* 2015 Rapid increase in cosmogenic ^{14}C in AD 775 measured in New Zealand kauri trees indicates short-lived increase in ^{14}C production spanning both hemispheres. *Earth Planet. Sci. Lett.* **411**, 290–297.
96. Dormand JR, Prince PJ. 1980 A family of embedded Runge-Kutta formulae. *J. Comput. Appl. Math.* **6**, 19–26. (doi:10.1016/0771-050x(80)90013-3)

Downloaded from https://royalsocietypublishing.org/ on 31 October 2022

97. Kidger P. 2021 *On neural differential equations*. Oxford, UK: University of Oxford.
98. Betancourt M. 2017 A conceptual introduction to hamiltonian Monte Carlo. (http://arxiv.org/abs/1701.02434)
99. Willner SN, Hartin C, Gieseke R. 2017 pyhector: a Python interface for the simple climate model Hector. *J. Open Sourc. Softw.* **2**, 248. (doi:10.21105/joss.00248)
100. Gieseke R, Willner SN, Mengel M. 2018 Pymagicc: a Python wrapper for the simple climate model MAGICC. *J. Open Sourc. Softw.* **3**, 516. (doi:10.21105/joss.00516)
101. Metropolis N, Rosenbluth AW, Rosenbluth MN, Teller AH, Teller E. 1953 Equation of state calculations by fast computing machines. *J. Chem. Phys.* **21**, 1087–1092.
102. Ramsey CB. 1995 Radiocarbon calibration and analysis of stratigraphy: the OxCal program. *Radiocarbon* **37**, 425–430.
103. Ramsey CB, Lee S. 2013 Recent and planned developments of the program OxCal. *Radiocarbon* **55**, 720–730.
104. Buck CE, Christen A, James GN. 1999 BCal: an on-line Bayesian radiocarbon calibration tool. *Internet Archaeol.* **7**.
105. Lougheed BC, Obrochta SP. 2016 MatCal: open source Bayesian ^{14}C age calibration in Matlab. *J. Open Res. Softw.* **4**, e42. (doi:10.5334/jors.130)
106. Lanos P, Dufresne P. 2019 ChronoModel version 2.0 User manual.
107. Goodman J, Weare J. 2010 Ensemble samplers with affine invariance. *Commun. Appl. Math. Comput. Sci.* **5**, 65–80.
108. Skilling J. 2004 Nested sampling. In *Bayesian Inference and Maximum Entropy Methods in Science and Engineering: 24th Int. Workshop on Bayesian Inference and Maximum Entropy Methods in Science and Engineering*, (eds R Fischer, R Preuss, UV Toussaint), vol. 735, pp. 395–405. American Institute of Physics Conference Series.
109. Williams CK, Rasmussen CE. 2006 *Gaussian processes for machine learning*. Cambridge, MA: MIT press.
110. Foreman-Mackey D, Yadav S, Tronsgaard R. 2022 theorashid. dfm/tinygp: tinygp v0.2.1. Zenodo. (doi:10.5281/zenodo.6389738)
111. Usoskin IG, Kromer B. 2005 Reconstruction of the ^{14}C production rate from measured relative abundance. *Radiocarbon* **47**, 31–37.
112. Uusitalo J *et al.* 2018 Solar superstorm of AD 774 recorded subannually by Arctic tree rings. *Nat. Commun.* **9**, 1–8. (doi:10.1038/s41467-018-05883-1)
113. Rakowski AZ, Krąpiec M, Huels M, Pawlyta J, Boudin M. 2018 Increase in radiocarbon concentration in tree rings from Kujawy village (se poland) around AD 993–994. *Radiocarbon* **60**, 1249–1258.
114. Miyake F, Hakozaki M, Kimura K, Tokanai F, Nakamura T, Takeyama M, Moriya T. 2022 Regional differences in carbon-14 data of the 993 CE cosmic ray event. *Front. Astron. Space Sci.* **9**, 139. (doi:10.3389/fspas.2022.886140)
115. McDonald L, Chivall D, Miles D, Bronk Ramsey C. 2019 Seasonal variations in the ^{14}C content of tree rings: influences on radiocarbon ralibration and single-year curve construction. *Radiocarbon* **61**, 185–194.
116. Park JH, Southon J, Seo JW, Creasman PP, Hong W, Park G, Sung KH. 2021 Δ ^{14}C peaks appearing in earlywood and latewood tree rings (AD 770–780) in northeastern Arizona. *Radiocarbon* **63**, 223–228.
117. Kromer B, Manning SW, Kuniholm PI, Newton MW, Spurk M, Levin I. 2001 Regional $^{14}CO_2$ offsets in the troposphere: magnitude, mechanisms, and consequences. *Science* **294**, 2529–2532.
118. Wacker L *et al.* 2020 Findings from an in-depth annual tree-ring radiocarbon intercomparison. *Radiocarbon* **62**, 873–882.
119. Mölder F *et al.* 2021 Sustainable data analysis with Snakemake [version 2; peer review: 2 approved]. *F1000Research* **10**.
120. Miyake F. 2013 *Reconstruction of cosmic-ray intensity in the past from measurements of radiocarbon in tree rings*. Nagoya, Japan: Nagoya University.
121. Paleari CI *et al.* 2022 Cosmogenic radionuclides reveal an extreme solar particle storm near a solar minimum 9125 years BP. *Nat. Commun.* **13**, 1–9. (doi:10.1038/s41467-021-27891-4)
122. Phan D, Pradhan N, Jankowiak M. 2019 Composable effects for flexible and accelerated probabilistic programming in NumPyro. (http://arxiv.org/abs/1912.11554)
123. Zhang Q, Sharma U, Dennis JA, Scifo A, Kuitems M, Büntgen U, Owens MJ, Dee MW, Pope BJS. 2022 Modelling cosmic radiation events in the tree-ring radiocarbon record. *Figshare*.

124. Pérez F, Granger BE. 2007 IPython: a system for interactive scientific computing. *Comput. Sci. Eng.* **9**, 21–29.
125. Der Walt Van S, Colbert SC, Varoquaux G. 2011 The NumPy array: a structure for efficient numerical computation. *Comput. Sci. Eng.* **13**, 22–30.
126. Hunter JD. 2007 Matplotlib: a 2D graphics environment. *Comput. Sci. Eng.* **9**, 90–95.
127. Jones E, Oliphant T, Peterson P, Others. 2001 SciPy: open source scientific tools for Python. See www.scipy.org/.
128. Hinton SR. 2016 ChainConsumer. *J. Open Sourc. Softw.* **1**, 00045. (doi:10.21105/joss.00045)

Downloaded from https://royalsocietypublishing.org/ on 31 October 2022